

CLM3.5 Documentation

¹K. W. Oleson, ²G.-Y. Niu, ²Z.-L. Yang, ¹D.M. Lawrence, ¹P. E. Thornton, ³P.J. Lawrence, ⁴R.
Stockli, ⁵R.E. Dickinson, ¹G.B. Bonan, ¹S. Levis

¹Climate and Global Dynamics Division
National Center for Atmospheric Research
Boulder, Colorado

²Department of Geological Sciences
The University of Texas at Austin
Austin, Texas

³Cooperative Institute for Research in Environmental Sciences
University of Colorado
Boulder, CO

⁴Department of Atmospheric Science
Colorado State University
Fort Collins, CO

⁵Georgia Institute of Technology
Atlanta, Georgia

Corresponding Author:
Keith Oleson
National Center for Atmospheric Research
PO Box 3000
Boulder, CO 80307-3000
oleson@ucar.edu
Phone: 303-497-1332
FAX: 303-497-1695

April, 2007

1. Introduction

The circulation of water through the Earth system is of critical importance to life on Earth. The hydrological cycle is also intimately linked to the energy cycle and to biogeochemical processes including the carbon cycle. Simulating the various processes that interact to form the hydrological cycle is a daunting task for climate models. In particular, over land, interactions between precipitation and the vegetation/soil system determine the partitioning of water into various storage reservoirs and the subsequent release of water vapor to the atmosphere. Successful simulation of these interactions by the land surface component of a climate model requires detailed representation of processes such as interception, throughfall, canopy drip, snow accumulation and ablation, infiltration, surface and sub-surface runoff, soil moisture, and the partitioning of evapotranspiration between canopy evaporation, transpiration, and soil evaporation. Depending on the capabilities of the model, the water cycle components may interact with and affect the simulation of biogeochemical processes such as the carbon and nitrogen cycle, dust and trace gas emissions, water and carbon isotopes, and vegetation dynamics.

The Community Land Model version 3 (CLM3) is a computer model that represents land surface processes within the context of global climate simulation (Oleson et al. 2004). Dickinson et al. (2006) described the climate statistics of CLM3 when coupled to the Community Climate System Model (CCSM3) (Collins et al. 2006). Hack et al. (2006) provided an analysis of selected features of the land hydrological cycle. Bonan and Levis (2006) evaluated global plant biogeography and net primary production from CLM3 when coupled to a dynamic global vegetation model (DGVM). Lawrence et al. (2007) examined the impact of changes in CLM3 hydrological parameterizations on partitioning of evapotranspiration (ET) and its effect on the

timescales of ET response to precipitation events, interseasonal soil moisture storage, soil moisture memory, and land-atmosphere coupling. Although the simulation of land surface climate by CLM3 is in many ways adequate (Dickinson et al. 2006), many of the more unsatisfactory aspects of the simulated climate described in these studies can be traced directly to a deficient simulation of the hydrological cycle.

A poor simulation of the hydrological cycle in the Amazon basin is indicative of the hydrologic deficiencies in CLM3. Here, the simulated present-day climate is biased warm and dry with lower runoff than observed (Dickinson et al. 2006). In part this is due to insufficient precipitation from the atmospheric model but is exacerbated by unrealistic partitioning of ET and deficiencies in runoff and soil water storage (Dickinson et al. 2006, Lawrence et al. 2007, Hack et al. 2006). In particular, these studies indicate the simulated evapotranspiration is dominated by soil and canopy evaporation instead of by transpiration as observed. These biases result in a poor simulation of vegetation biogeography with much less broadleaf evergreen trees and more deciduous trees than observed (Bonan and Levis 2006). On a global scale, forest cover is underestimated compared to observations in favor of grasses because of dry soils. Lawrence and Chase (2007) noted that because of the unrealistic partitioning of ET, improved surface datasets of leaf and stem area index and plant functional type had unexpectedly limited success in rectifying temperature and precipitation biases in the coupled modeling system. Other hydrology-related problems in the model include low gross primary production (GPP) (Dickinson et al. 2006) and poor simulation of the magnitude and seasonality of runoff and soil water storage in regions with frozen soil (Niu and Yang 2006).

One advantage of a community model is that there are a significant number of scientists willing to scrutinize its scientific contents, offer constructive criticism, and improve its

performance. Several new parameterizations designed to address these specific deficiencies in CLM have been proposed (Niu et al. 2005, Niu and Yang 2006, Niu et al. 2007, Thornton and Zimmerman 2007, Lawrence and Chase 2007, Lawrence et al. 2007). Validation and sensitivity testing of the individual parameterizations have been addressed by the respective authors. While these parameterizations have individually been shown to be clearly beneficial in alleviating specific biases in the model, it is not clear how they might interact with each other and what the net effects on the simulation of the hydrological cycle might be. In Oleson et al. (2007) we report on the aggregated effects on simulated climate at a global scale both uncoupled and coupled to an atmospheric model. We show that in general the new parameterizations result in a more realistic depiction of the hydrologic cycle. We also demonstrate that the improved hydrology translates into better simulation of GPP and present-day vegetation biogeography. However, the simulation of hydrology in certain regions remains problematical. Stockli et al. (2007) further examine the performance of the new model in the context of tower flux observations.

2. Material and Methods

2.1. CLM3

CLM3 is the land surface component of CCSM3, a community-developed global climate model applied to studies of interannual and interdecadal variability, paleoclimate regimes, and projections of future climate change (Collins et al. 2006). The land surface is described by several plant functional types (PFTs) which differ in their ecological and hydrological characteristics and by soil texture types which determine the thermal and hydrologic properties of soils. Biophysical processes simulated by CLM3 include solar and longwave radiation interactions with vegetation canopy and soil, momentum and turbulent fluxes from canopy and

soil, heat transfer in soil and snow, hydrology of canopy, soil, and snow, and stomatal physiology and photosynthesis. A detailed description of how these processes are parameterized in CLM3 can be found in Oleson et al. (2004). Specific detail on the parameterizations relevant to this paper is provided in the next section.

2.2. Summary of model improvements

We implemented new surface datasets and parameterizations within CLM3. The modifications consist of surface datasets based on Moderate Resolution Imaging Spectroradiometer (MODIS) products (Lawrence and Chase 2007), an improved canopy integration scheme (Thornton and Zimmermann 2007), scaling of canopy interception (Lawrence et al. 2007), a simple TOPMODEL-based model for surface and sub-surface runoff (Niu et al. 2005), a simple groundwater model for determining water table depth (Niu et al. 2007), and a new frozen soil scheme (Niu and Yang 2006). In this paper, we also describe four additional modifications. Three of these, an improved description of soil water availability, a resistance term to reduce excessive soil evaporation, and the introduction of a factor to simulate nitrogen limitation on plant productivity, can be categorized as new or improved parameterizations from the perspective of CLM3. The other may be categorized as fixing an algorithmically defective existing parameterization (Dickinson et al. 2006). In this section, we provide a brief overview of these modifications and summarize their individual effects on simulated hydrology and climate. More detailed descriptions of the parameterizations and assessments of their performance can be found in the cited papers. However, we provide full details in Appendix A-G in order to fully document the new aspects of the model as compared to CLM3. The new model has been designated as CLM3.5.

2.2.1. Surface Datasets

Surface datasets of PFT and leaf and stem area index (LAI and SAI) in CLM3 are based on one year of data from the Advanced Very High Resolution Radiometer (AVHRR) (Bonan et al. 2002). Lawrence and Chase (2007) developed new surface datasets for CLM3 that better reproduce the physical properties described in the multi-year MODIS land surface data products compared to the CLM3 representation. Specifically, new PFT, glacier, and wetland maps, and LAI, SAI and soil color (which determines soil albedo) datasets were created. Lawrence and Chase (2007) documented some improvements in simulated surface albedo, near-surface temperature, and precipitation. As noted above however, the hydrologic deficiencies in the model limited the effectiveness of these improvements, the issue that we address in this paper. We have replaced the 0.5° resolution datasets used in CLM3 with these new datasets. The surface datasets used in this study were generated at the desired spatial resolution based on area-weighted averaging of the 0.5° data.

2.2.2. Canopy Integration

Although the vegetation canopy in CLM3 is divided into shaded and sunlit fractions, all the direct and diffuse canopy intercepted radiation is assigned to the sunlit canopy fraction. Thornton and Zimmerman (2007) combined a logical framework relating the structural and functional characteristics of a vegetation canopy and a true two-leaf canopy model to produce a canopy integration scheme for land surface models. The framework posits a linear relationship between the ratio of leaf area to leaf mass (specific leaf area) and overlying leaf area index within the canopy. An inconsistency in the treatment of canopy radiation in CLM3 was also corrected. Incorporation of the new scheme in CLM3 resulted in significant increases in global GPP in both offline and coupled simulations. In separate simulations performed by us, we

observed that the large increase in production was accompanied by a large depletion in soil moisture in some regions because of increases in transpiration rates (not shown). In other words the improvement in GPP was limited by the dry soils in CLM3. This provided additional motivation to complement the canopy integration scheme with a more realistic description of hydrology. Here, we implemented the canopy integration scheme in diagnostic canopy mode (using the remotely-sensed LAI climatology from Lawrence and Chase (2007)) exactly as described in Thornton and Zimmerman (2007).

2.2.3. Canopy Interception

The canopy in CLM3 intercepts too much water (Hack et al. 2006). This limits transpiration rates because only the dry fraction of the canopy can transpire and atmospheric evaporative demand is mostly met by the evaporation of the intercepted water. A factor is implemented that scales the parameterization of interception from point to grid cell (Lawrence et al. 2007) (Appendix A). This results in lower canopy interception rates and increases the amount of water reaching the soil surface and consequently improves the ET partitioning (Lawrence et al. 2007).

2.2.4. Surface and Subsurface Runoff

The runoff scheme in CLM3 is a combination of the TOPMODEL (Beven and Kirkby 1979) and BATS (Dickinson et al. 1993) parameterizations. Niu et al. (2005) showed that this scheme overestimates the runoff peaks and underestimates runoff in recession periods resulting in low modeling efficiency, mainly because of the high ratio of surface runoff to total runoff. They introduced a simple TOPMODEL-based runoff scheme (SIMTOP) that mitigated several problems associated with implementing the TOPMODEL approach within a climate model. A key concept underlying their approach is that of fractional saturated area, which is determined by the topographic characteristics and soil moisture state of a grid cell. The topographic data is

simplified to a single topographic parameter, the potential or maximum fractional saturated area, which is determined from coarse resolution Digital Elevation Model (DEM) data. Surface runoff is parameterized in terms of the saturated fraction and an exponential function of water table depth. The scheme also accounts for infiltration excess which is an additional mechanism by which surface runoff can be generated. Subsurface runoff is a product of an exponential function of the water table depth and a single coefficient for maximum subsurface runoff. Niu et al. (2005) demonstrated that modeling efficiency of runoff for a small watershed using SIMTOP was much improved compared to CLM3. Global experiments with the new scheme showed significant improvement in the magnitude and timing of runoff, particularly in tropical and arid regions. We implemented SIMTOP in CLM3 as described in Appendix B.

2.2.5. Groundwater and Water Table Depth

In the original SIMTOP (Niu et al. 2005), the assumptions made to derive the water table depth restricted the applicability of the formulation to regions where the water table is relatively shallow and times when the water table is in approximate equilibrium with the model soil moisture. A simple lumped aquifer model was suggested by Niu et al. (2005) as a way to extend the SIMTOP approach to cases when the water table is deeper than the bottom of the model soil column. Furthermore, groundwater influences soil moisture and runoff generation and hence surface energy and water balances, making it desirable to include a groundwater component in land surface models. A simple groundwater model (SIMGM) was developed by Niu et al. (2007) to address these issues. The model represents groundwater recharge and discharge processes through a dynamic coupling between the bottom soil layer and an unconfined aquifer. The aquifer is added as a single integration element below the soil column (Figure C1). Niu et al. (2007) found that the modeled water storage anomaly compared favorably to the water

storage anomaly estimated by the Gravity Recovery And Climate Experiment (GRACE) satellites for several river basins. SIMGM is implemented as described in Appendix C.

2.2.6. Frozen Soil

Although experiments with SIMTOP conducted by Niu et al. (2005) demonstrated improvement in the magnitude and timing of runoff in tropical and arid regions, significant improvements were not apparent in arctic and boreal regions. This was attributed to deficiencies in the treatment of frozen soil in CLM3. Niu and Yang (2006) demonstrated that in these regions CLM3 soil has low permeability to water which results in larger and earlier springtime runoff peaks than observed. The introduction of the concepts of supercooled soil water and fractional impermeable area into CLM3 and the parameterization of soil hydraulic properties as a function of impermeable area were shown to increase infiltration rates and improve the simulation of runoff in cold-region river basins of various spatial scales. In other similar experiments with CLM3, Decker and Zeng (2006) and Yi et al. (2006) showed improvements in their simulations by accounting for supercooled soil water. The parameterizations described in Niu and Yang (2006) were implemented as described in Appendix D.

2.2.7. Soil Water Availability

Plant water stress in CLM3 is linked to root distribution and soil matric potential which serves as a surrogate for negative leaf water potential. Root distribution is semi-unique for each PFT (Oleson et al. 2004), however, both the matric potential at which the initial reduction in stomatal conductance occurs (ψ_{open}) and the potential at which final reduction occurs (ψ_{close}) (leaf desiccation) are prescribed as constants for all PFTs ($\psi_{close} = -1.5 \times 10^5$ mm, $\psi_{open} = \psi_{sat}$ where ψ_{sat} is saturated matric potential, which varies by soil texture but not PFT). This is in contrast to numerous field studies that show that PFTs have unique values of ψ_{open} and ψ_{close}

(e.g., as summarized by White et al. 2000). Furthermore, since $\psi_{open} = \psi_{sat}$ in CLM3, plant water stress begins to occur immediately at soil moisture levels less than saturation. We implemented a parameterization for plant water stress that is functionally similar to that in CLM3 but allows for PFT variability in ψ_{open} and ψ_{close} using values from White et al. (2000) which lowers the soil moisture levels at which stress begins to occur (Appendix E). The new parameterization results in increased soil water availability for plants.

In CLM3, only soil layers with a temperature greater than the freezing temperature of fresh water (273.16K) can supply water to plants. This ignores the fact that significant amounts of liquid water may co-exist with ice at freezing temperature. Furthermore, the introduction of the supercooled soil water concept means that liquid water can exist at temperatures below freezing. The dependence of plant water stress on temperature has been removed in the new formulation (Appendix E).

2.2.8. Soil Evaporation

Lawrence et al. (2007) found that even after implementing alterations to CLM3 to improve ET partitioning, soil evaporation was still an unreasonably large fraction of total ET. Similarly, preliminary simulations with the model changes discussed to this point yielded improved ET partitioning, however, the ratio of soil evaporation to total ET was still significantly larger than other model-based estimates of this fraction (e.g., as compared to the GSWP2 multi-model ensemble (Dirmeyer et al. 2006) or to Choudhury et al. (1998)). Lawrence et al. (2007) reduced soil evaporation in their CLM3 experiments by altering two parameters in the formulation for the turbulent transfer coefficient between the soil and the canopy air. They noted, however, that although this reduced soil evaporation, sensible heat flux was also reduced such that soil temperatures increased. Further testing of this approach by us in the context of land cover

change experiments revealed that surface soil temperatures were unrealistically sensitive to changes in leaf and stem area (not shown). In certain regions, the air temperature response to changes in land cover types was largely controlled by this behavior. Here, we retained the turbulent transfer coefficient as formulated in CLM3 and instead added a soil resistance term that depends on soil moisture and thus affects only the soil latent heat flux. Justification and details of this parameterization are provided in Appendix F. This approach reduces evaporation from the soil, resulting in better ET partitioning and improves the simulation of surface fluxes (Stockli et al. 2007).

2.2.9. Other Modifications

Concurrent with development of the biophysical aspects of CLM3 discussed above, extensive efforts are ongoing to introduce the effects of biogeochemistry into the model. More specifically, the option to include a prognostic treatment of carbon and nitrogen cycle dynamics has been implemented (CLM-CN, Thornton and Zimmerman 2007, Thornton et al. 2007). The inclusion of the carbon/nitrogen cycle in conjunction with most of the changes described above results in reasonable prognostic simulations of leaf area index and plant productivity (Thornton et al. 2007). However, there are many applications for which including the full carbon/nitrogen cycle is neither practical nor desirable. In these cases, the model is over productive because of the lack of nitrogen limitation on plant productivity. To overcome this, a simple approach is adopted that applies a PFT-dependent foliage nitrogen limitation factor to limit the maximum rate of carboxylation attainable by the PFT. More details can be found in Appendix G and Table G1. A separate set of factors is suggested for the Dynamic Global Vegetation Model (DGVM) (Levis et al. 2004) (Table G1).

A dimensionless factor is prognostically determined in CLM3 that provides for a fractional reduction in snow albedo due to snow aging (assumed to represent increasing grain size and dirt, soot content). The implementation of this algorithm in the code was found to be deficient and has been corrected (Y.-J. Dai, personal communication). The effect of this is to increase snow age thereby lowering snow albedo and resulting in earlier snow melt in certain regions (not shown).

Appendix A: Canopy Interception

The rate of water intercepted by the canopy ($\text{kg m}^{-2} \text{s}^{-1}$) is

$$q_{intr} = \alpha (q_{rain} + q_{sno}) \{1 - \exp[-0.5(L + S)]\} \quad (\text{A1})$$

where q_{rain} and q_{sno} are the liquid and solid precipitation rates ($\text{kg m}^{-2} \text{s}^{-1}$) and L and S are the exposed leaf and stem area index. The factor α has been changed from 1.0 to 0.25 to scale the interception from point to grid cell (Lawrence et al. 2007).

Appendix B: Surface and Sub-surface Runoff

The simple TOPMODEL-based runoff model (SIMTOP) described by Niu et al. (2005) is implemented. SIMTOP parameterizes surface runoff as consisting of overland flow from Dunne (runoff over saturated ground) and Horton (infiltration excess) mechanisms as

$$q_{over} = f_{sat} q_{liq,0} + (1 - f_{sat}) \max(0, q_{liq,0} - q_{infl,max}) \quad (\text{B1})$$

where $q_{liq,0}$ is liquid precipitation reaching the ground plus any melt water from snow ($\text{kg m}^{-2} \text{s}^{-1}$) and $q_{infl,max}$ is a maximum soil infiltration capacity ($\text{kg m}^{-2} \text{s}^{-1}$).

The variable f_{sat} is the saturated fraction of a grid cell. In Niu et al. (2005), f_{sat} was determined by the water table depth and the subgrid topographic characteristics of the grid cell and represented the potential or maximum saturated fraction (f_{max}). Niu and Yang (2006) modified the expression for f_{sat} to include a dependence on impermeable area fraction $f_{frz,1}$ of the top $i = 1$ soil layer (defined in Appendix D) as

$$f_{sat} = (1 - f_{frz,1}) f_{max} \exp(-0.5 f_{z_{\nabla}}) + f_{frz,1} \quad (\text{B2})$$

where f_{\max} is the maximum saturated fraction, f is a decay factor (m^{-1}), and z_{∇} is the water table depth (m). The decay factor f for global simulations was determined through sensitivity analysis and comparison with observed runoff to be 2.5 m^{-1} .

The maximum saturated fraction f_{\max} is defined as the discrete cumulative distribution function (CDF) of the topographic index when the grid cell mean water table depth is zero. Thus, f_{\max} is the percent of pixels in a grid cell whose topographic index is larger than or equal to the grid cell mean topographic index. It should be computed explicitly from the CDF at each grid cell at the resolution that the model is run. However, because this is a computationally intensive task for global applications, f_{\max} is calculated once from the CDF at 0.5 degree resolution following Niu et al. (2005) and then area-averaged to the desired resolution. The 0.5 degree resolution is compatible with resolution of the other CLM input surface datasets (e.g., plant functional types, leaf area index).

The maximum infiltration capacity in equation (B1) $q_{\text{infl},\max}$ is determined from soil texture and soil moisture (Entekhabi and Eagleson 1989) as

$$q_{\text{infl},\max} = k_{\text{sat},1} [1 + \nu(s - 1)]. \quad (\text{B3})$$

The liquid water content of the top soil layer relative to effective porosity and adjusted for saturated fraction is determined from

$$s = \frac{\frac{\theta_{\text{liq},1}}{\max(\theta_{\text{imp}}, \theta_{\text{sat},1} - \theta_{\text{ice},1})} - f_{\text{sat}}}{1 - f_{\text{sat}}} \quad (\text{B4})$$

where $\theta_{\text{liq},1}$ and $\theta_{\text{ice},1}$ are the volumetric liquid water and ice contents of the top soil layer, and $\theta_{\text{imp}} = 0.05$ is a minimum effective porosity. The variable ν is

$$v = -\left(\frac{d\psi}{ds}\right)_{s=1} \frac{1}{0.5\Delta z_1} \quad (\text{B5})$$

where Δz_1 is the thickness of the top soil layer (mm) and

$$\left(\frac{d\psi}{ds}\right)_{s=1} = -B_1 \psi_{sat,1} \cdot \quad (\text{B6})$$

The saturated hydraulic conductivity $k_{sat,1}$ ($\text{kg m}^{-2} \text{s}^{-1}$), volumetric water content at saturation (i.e., porosity) $\theta_{sat,1}$, exponent B_1 , and saturated soil matric potential $\psi_{sat,1}$ (mm) are determined from soil texture (% *sand*, % *clay*) (Oleson et al. 2004).

In Niu et al. (2005), the subsurface runoff or drainage q_{drai} ($\text{kg m}^{-2} \text{s}^{-1}$) was formulated as

$$q_{drai} = q_{drai,max} \exp(-fz_{\nabla}) \quad (\text{B7})$$

where $q_{drai,max} = 4.5 \times 10^{-4} \text{ kg m}^{-2} \text{ s}^{-1}$ is the maximum subsurface runoff when the grid-averaged water table depth is zero. To restrict drainage in frozen soils, Niu et al. (2005) added the following condition

$$q_{drai,max} \exp(-fz_{\nabla}) = 0 \quad \text{for } w_{ice,10} > w_{liq,10} \quad (\text{B8})$$

where $w_{ice,10}$ and $w_{liq,10}$ is the ice and liquid water content of the 10th soil layer (kg m^{-2}). In preliminary testing we found that a more gradual restriction of drainage was required so that the water table depth remained dynamic under partially frozen conditions. We implemented the following

$$q_{drai} = (1 - f_{imp}) q_{drai,max} \exp(-fz_{\nabla}) \quad (\text{B9})$$

where f_{imp} is the fraction of impermeable area determined from the ice content of the soil layers interacting with the water table

$$f_{imp} = \left\{ \exp \left[-\alpha \left(1 - \frac{\sum_i^{10} \frac{w_{ice,i}}{w_{ice,i} + w_{liq,i}} \Delta z_i}{\sum_i^{10} \Delta z_i} \right) \right] - \exp(-\alpha) \right\} \geq 0. \quad (B10)$$

where $\alpha = 3$ is an adjustable scale-dependent parameter, i is the index of the layer directly above the water table, and $w_{ice,i}$ and $w_{liq,i}$ are the ice and liquid water contents of soil layer i (kg m⁻²). This expression is functionally the same as that used to determine the permeability of frozen soil (Appendix D).

If the water table depth z_{∇} is below the soil column, then the drainage q_{drai} is removed from the aquifer (Appendix C). If z_{∇} is within the soil column, q_{drai} is extracted from the soil liquid water in soil layers within the water table (Appendix C). The value of $q_{drai,max}$ was determined from a calibration against the averaged observed water table depth for sixteen wells in Illinois (Niu et al. 2007). Future work will focus on optimizing spatially explicit values for parameters $q_{drai,max}$ and the decay factor f .

Two numerical adjustments are implemented to keep the liquid water content of each soil layer ($w_{liq,i}$) within physical constraints $0.01 \leq w_{liq,i} \leq (\theta_{sat,i} - \theta_{ice,i}) \Delta z_i$. These adjustments, $w_{liq}^{deficit}$ and w_{liq}^{excess} , may decrease or increase subsurface runoff, respectively. First, to help prevent negative $w_{liq,i}$, each layer is successively brought up to $w_{liq,i} = 0.01$ by taking the required amount of water from the layer below. If the total amount of water in the soil column is insufficient to accomplish this, the water is taken from the unconfined aquifer and the subsurface runoff ($w_{liq}^{deficit}$). Second, beginning with the bottom soil layer, any excess liquid water in each soil layer is successively added to the layer above. Any excess liquid water that remains after

saturation of the entire soil column (plus a maximum ponding depth $w_{liq}^{pond} = 10$ mm [Oleson et al. 2004]), w_{liq}^{excess} , is added directly to subsurface runoff. These two adjustments are rarely necessary.

Two other changes were made following Niu et al. (2005). First, the exponentially decaying saturated hydraulic conductivity was removed and replaced with a conductivity that depends on soil texture alone (Cosby et al. 1984). The saturated hydraulic conductivity is

$$k_{sat} = 0.0070556 \times 10^{-0.884+0.0153(\% sand)_i} \quad (B11)$$

where $(\% sand)_i$ is the sand content of the i^{th} soil layer.

Second, a no-drainage bottom boundary condition is imposed on the solution for soil moisture. Groundwater recharge (including gravitational drainage and upward flow driven by capillary forces) is now employed to update the bottom layer soil moisture (Appendix C). The coefficients of the tridiagonal set of equations for soil layer $i = 10$ (Equations (7.105) – (7.108) in Oleson et al. 2004) are now

$$a_i = -\frac{\partial q_{i-1}}{\partial \theta_{liq,i-1}} \quad (B12)$$

$$b_i = -\left[\frac{\partial q_{i-1}}{\partial \theta_{liq,i}} + \frac{\Delta z_i}{\Delta t} \right] \quad (B13)$$

$$c_i = 0 \quad (B14)$$

$$r_i = e_i + q_{i-1}^n. \quad (B15)$$

Appendix C: Groundwater and Water Table Depth

The determination of the water table depth z_v is based on work by Niu et al. (2007). In this approach, a groundwater component was added to CLM in the form of an unconfined aquifer

lying below the model soil column (Figure C1). The ground water solution is dependent on whether the water table is within or below the soil column. Two water stores are used to account for these solutions. The first, W_a , is the water stored in the unconfined aquifer (mm) and is proportional to the change in water table depth when the water table z_v is below the lower boundary of the model soil column (3.43 m). The second, W_t , is the actual groundwater which can be within the soil column. When the water table is below the soil column, $W_t = W_a$. When the water table is within the soil column, W_a is constant because there is no water exchange between the soil column and the underlying aquifer, while W_t varies with soil moisture conditions. W_a , W_t , and z_v are prognostic variables within the model.

For the case when the water table is below the soil column, the temporal variation of the water stored in the unconfined aquifer W_a (mm) is

$$\frac{dW_a}{dt} = q_{recharge} - q_{drai} \quad (C1)$$

where $q_{recharge}$ is the recharge to the aquifer ($\text{kg m}^{-2} \text{s}^{-1}$) and the subsurface runoff q_{drai} is equivalent to the groundwater discharge. The recharge rate is derived from Darcy's law and is defined as positive when water enters the aquifer

$$q_{recharge} = -k_a \frac{-10^3 z_v - (\psi_{10} - 10^3 z_{10})}{10^3 (z_v - z_{10})} \quad (C2)$$

where k_a is the hydraulic conductivity of the aquifer ($\text{kg m}^{-2} \text{s}^{-1}$), z_v is the water table depth (m), and ψ_{10} is the matric potential of the bottom (10th) soil layer (mm) at the node depth $z_{10} = 2.865$ m. The matric potential of the bottom soil layer is determined from

$$\psi_{10} = \psi_{sar,10} (s_{10})^{-B_{10}} \quad (C3)$$

where $\psi_{sat,10}$ and B_{10} are the saturated matric potential (mm) and soil texture-dependent Clapp and Hornberger (1978) exponent for the bottom soil layer. The wetness of the bottom soil layer $0.01 < s_{10} < 1$ is determined from the volumetric liquid water content $\theta_{liq,10}$ and effective porosity $\theta_{sat,10} - \theta_{ice,10} \geq 0$

$$s_{10} = \frac{\theta_{liq,10}}{\theta_{sat,10} - \theta_{ice,10}}. \quad (C4)$$

The hydraulic conductivity below the model soil column is assumed to decay with depth from the hydraulic conductivity of the bottom layer ($k_{10} \exp[-f(z - z_{10})]$). Thus, the hydraulic conductivity of the aquifer is

$$k_a = \frac{k_{10} \{1 - \exp[-f(z_v - z_{10})]\}}{f(z_v - z_{10})}. \quad (C5)$$

where k_{10} is the hydraulic conductivity of the bottom layer ($\text{kg m}^{-2} \text{s}^{-1}$).

The water table depth is calculated from the aquifer water storage scaled by the average specific yield $S_y = 0.2$ (the fraction of water volume that can be drained by gravity in an unconfined aquifer)

$$z_v = z_{h,10} + 25 - \frac{W_a}{10^3 S_y} \quad (C6)$$

where $z_{h,10}$ is the depth of the bottom of the soil column (3.43 m). The form of equation (C6) originates from the assumption that the initial amount of water in the aquifer is 4800 mm and the corresponding initial water table depth is 1 m below the bottom of the soil column. The water table depth is at the bottom of the soil column ($z_v = z_{h,10}$) when the aquifer water is at its prescribed maximum value (5000 mm). The change in soil water in the bottom layer is

$$\Delta W_{liq,10} = -q_{recharge}\Delta t + \max(0, W_a - 5000) \quad (C7)$$

where Δt is the model time step (s).

For the case when the water table is within the model soil column, there is no water exchange between the soil column and the underlying aquifer. However, variations of the water table depth are still computed from equations (C1) and (C2), but the variables of the bottom layer are replaced with those of the layer directly above the water table. Hence,

$$\frac{dW_t}{dt} = q_{recharge} - q_{drai}. \quad (C8)$$

The recharge rate is

$$q_{recharge} = -k_i \frac{(\psi_{sat,i+1} - 10^3 z_{\nabla}) - (\psi_i - 10^3 z_i)}{10^3 (z_{\nabla} - z_i)} \quad (C9)$$

where $\psi_{sat,i+1} - 10^3 z_{\nabla}$ is the water head at the water table depth and i is the index of the layer directly above the water table.

In Niu et al. (2007), the water table depth is computed from equation (C6) but with the specific yield determined by the volume of air pores (the pore space not filled with water) within the soil to convert W_t to water table depth. In preliminary global simulations we found that this approach resulted in unstable water table calculations for a significant proportion of grid cells. More specifically, when repeatedly forcing the model with a single year of atmospheric data, the temporal evolution of water table depth was significantly different from year to year for some grid cells, with occasional rapid (within a few days) movement of the water table depth to the soil surface in some cases. This occurred in grid cells with soil water contents near saturation because of the small amount of available pore space. This had deleterious implications for stability of surface fluxes and temperature. For example, we found that 4% of the grid cells

would not satisfy the imposed spinup criterion (year to year change in annual mean surface fluxes less than 0.1 W m^{-2} (Yang et al. 1995). Here, we implement a calculation based on effective porosity only. Although less defensible from a physical viewpoint, the new approach stabilizes the water table calculation for these grid cells and eliminates unrealistic oscillations in surface fluxes and temperature. The spinup criterion is now satisfied for more than 99% of the grid cells in a global simulation within 30 years after starting the model from arbitrary initial conditions. The water table depth calculation is then

$$z_{\nabla} = \left\{ \begin{array}{l} z_{h,i+1} - \left[\frac{W_t - 10^3 \times 25S_y - \sum_{j=i+2}^{10} \Delta z_j (\theta_{sat,j} - \theta_{ice,j})}{10^3 (\theta_{sat,i+1} - \theta_{ice,i+1})} \right] \quad 1 \leq i \leq 8 \\ z_{h,i+1} - \left[\frac{W_t - 10^3 \times 25S_y}{10^3 (\theta_{sat,i+1} - \theta_{ice,i+1})} \right] \quad i = 9 \end{array} \right\}. \quad (\text{C10})$$

where θ_{ice} is the volumetric ice content of a layer and i is the index of the layer directly above the water table. In this case, the subsurface runoff q_{drai} is extracted from the soil liquid water in layers within the water table instead of from the aquifer. The partitioning of discharge to these layers is proportional to the layer depth-weighted hydraulic conductivity as

$$\Delta w_{liq,j} = - \frac{q_{drai} k_j \Delta t \Delta z_j}{\sum_{j=i+1}^{10} k_j \Delta z_j} \quad j = i + 1, 10 \quad (\text{C11})$$

where Δt is the time step (s) and i is the index of the layer directly above the water table.

Appendix D: Frozen Soil

The heat conduction equation is solved numerically to calculate the soil and snow temperatures for a ten-layer soil column with up to five overlying layers of snow (Oleson et al.

2004). The temperature profile is calculated first without phase change and then readjusted for phase change. Melting is still treated as in CLM3 (Oleson et al. 2004). Melting occurs if

$$T_i > T_f \text{ and } w_{ice,i} > 0 \quad (\text{D1})$$

where T_i and $w_{ice,i}$ are the soil temperature (K) and ice content (kg m^{-2}) of layer i , and T_f is freezing temperature (K). The amount of ice that is melted is assessed from the energy needed to change T_i to T_f .

For the freezing process, Niu and Yang (2006) incorporated the concept of supercooled soil water in CLM. The supercooled soil water is the liquid water that coexists with ice over a wide range of temperatures below freezing and is implemented through a freezing point depression equation

$$w_{liq,max,i} = \Delta z_i \theta_{sat,i} \left[\frac{10^3 L_f (T_f - T_i)}{g T_i \psi_{sat,i}} \right]^{-1/B_i} \quad T_i < T_f \quad (\text{D2})$$

where $w_{liq,max,i}$ is the maximum liquid water in layer i (kg m^{-2}) when the soil temperature T_i is below the freezing temperature T_f , L_f is the latent heat of fusion (J kg^{-1}), and g is the gravitational acceleration (m s^{-2}). Freezing occurs if

$$T_i < T_f \text{ and } w_{liq,i} > w_{liq,max,i}. \quad (\text{D3})$$

The ice content at model step $n + 1$ is calculated from

$$w_{ice,i}^{n+1} = \left\{ \begin{array}{ll} \min \left(w_{liq,i}^n + w_{ice,i}^n - w_{liq,max,i}^n, w_{ice,i}^n - \frac{H_i \Delta t}{L_f} \right) & w_{liq,i}^n + w_{ice,i}^n \geq w_{liq,max,i}^n \\ 0 & w_{liq,i}^n + w_{ice,i}^n < w_{liq,max,i}^n \end{array} \right\} \quad (\text{D4})$$

where H_i is the amount of energy needed to change T_i to T_f ($H_i < 0$) (Oleson et al. 2004).

Because part of the energy H_i may not be released in freezing, the energy is recalculated as

$$H_{i*} = H_i - \frac{L_f (w_{ice,i}^n - w_{ice,i}^{n+1})}{\Delta t} \quad (D5)$$

and the energy H_{i*} is used to cool the soil layer.

The impermeable fraction $f_{frz,i}$ (used in equation (B2) to determine the saturated fraction of the grid cell) is parameterized as a function of soil ice content (Niu and Yang 2006)

$$f_{frz,i} = \left\{ \exp \left[-\alpha \left(1 - \frac{w_{ice,i}}{w_{ice,i} + w_{liq,i}} \right) \right] - \exp(-\alpha) \right\} \geq 0 \quad (D6)$$

where $\alpha = 3$ is an adjustable scale-dependent parameter, and $w_{ice,i}$ and $w_{liq,i}$ are the ice and liquid water contents of soil layer i (kg m^{-2}). The hydraulic properties of the soil are also modified. The hydraulic conductivity is defined at the depth of the interface of two adjacent layers $z_{h,i}$ (m) and is a function of the saturated hydraulic conductivity $k_{sat} [z_{h,i}]$, the volumetric soil moisture of the two layers, and the impermeable fraction

$$k [z_{h,i}] = \left\{ \begin{array}{l} \left[1 - 0.5 (f_{frz,i} + f_{frz,i+1}) \right] k_{sat} [z_{h,i}] \left[\frac{0.5 (\theta_i + \theta_{i+1})}{0.5 (\theta_{sat,i} + \theta_{sat,i+1})} \right]^{2B_i+3} \quad 1 \leq i \leq 9 \\ (1 - f_{frz,i}) k_{sat} [z_{h,i}] \left[\frac{\theta_i}{\theta_{sat,i}} \right]^{2B_i+3} \quad i = 10 \end{array} \right\} \quad (D7)$$

where θ is the total (ice plus liquid) volumetric soil moisture. The soil matric potential is determined from the total water content as

$$\psi_i = \psi_{sat,i} \left(\frac{\theta_i}{\theta_{sat,i}} \right)^{-B_i} \geq -1 \times 10^8 \quad 0.01 \leq \frac{\theta_i}{\theta_{sat,i}} \leq 1 \quad (D8)$$

Appendix E: Soil Moisture Availability

The effect of soil moisture stress on plant transpiration and photosynthesis is parameterized through a soil moisture limitation function acting on the leaf-scale maximum carboxylation capacity of Rubisco (Thornton and Zimmerman 2007). The limitation function is

$$\beta_t = \sum_i w_i r_i \quad (\text{E1})$$

where w_i is a soil dryness or plant wilting factor for soil layer i and r_i is the fraction of roots in layer i (Oleson et al. 2004). The plant wilting factor w_i is

$$w_i = \left\{ \begin{array}{l} \left(\frac{\theta_{sat,i} - \theta_{ice,i}}{\theta_{sat,i}} \right) \left(\frac{\psi_i - \psi_{close}}{\psi_{open} - \psi_{close}} \right) \leq 1 \\ 0 \end{array} \right. \left. \begin{array}{l} \theta_{liq,i} > 0 \\ \theta_{liq,i} = 0 \end{array} \right\} \quad (\text{E2})$$

The soil water matric potential ψ_i (mm) is

$$\psi_i = \psi_{sat,i} s_i^{-B_i} \geq \psi_{close} \quad (\text{E3})$$

Soil wetness s_i is defined as

$$s_i = \frac{\theta_{liq,i}}{\theta_{sat,i} - \theta_{ice,i}} \geq 0.01. \quad (\text{E4})$$

where $\theta_{liq,i} \leq \theta_{sat,i} - \theta_{ice,i}$. The wilting point potential (full stomatal closure) ψ_{close} and the potential at which the stomata are fully open ψ_{open} (both in mm) are PFT-dependent parameters defined in Table E1.

Appendix F: Soil Evaporation

For vegetated surfaces, the water vapor flux from the soil beneath the canopy E_g ($\text{kg m}^{-2} \text{s}^{-1}$) is

$$E_g = -\rho_{atm} \frac{(q_s - q_g)}{r_{aw}'} \quad (\text{F1})$$

where q_s is the specific humidity of air at height $z_{0w} + d$ (the canopy air specific humidity), and r_{aw}' is the aerodynamic resistance ($s\ m^{-1}$) to water vapor transfer between the ground at height z_{0w}' and the canopy air at height $z_{0w} + d$ (water vapor roughness length plus displacement height (m)).

The specific humidity of the soil surface q_g is assumed to be proportional to the saturation specific humidity

$$q_g = \alpha q_{sat}^T \quad (F2)$$

where q_{sat}^T is the saturated specific humidity at the ground surface temperature T_g . The factor α is a weighted combination of values for soil and snow

$$\alpha = \alpha_{soi,1} (1 - f_{sno}) + \alpha_{sno} f_{sno} \quad (F3)$$

where f_{sno} is the fraction of ground covered by snow, and $\alpha_{sno} = 1.0$. $\alpha_{soi,1}$ refers to the surface soil layer and is a function of the surface soil water matric potential ψ as in Philip (1957)

$$\alpha_{soi,1} = \exp\left(\frac{\psi_1 g}{10^3 R_{wv} T_g}\right) \quad (F4)$$

where R_{wv} is the gas constant for water vapor ($J\ kg^{-1}\ K^{-1}$), g is the gravitational acceleration ($m\ s^{-2}$), and ψ_1 is the soil water matric potential of the top soil layer ($kg\ m^{-2}$).

The term α is supposed to be the air relative humidity at the humidity roughness height z_{0w}' . As pointed out by Kondo et al. (1990) and Wetzal and Chang (1987), however, the term frequently used is the relative humidity of the air adjacent to the water in the soil pore (i.e., the relationship from Philip (1957) is used in CLM), which is not the same as α . Some studies have found that the resistance to water vapor transport by molecular diffusion from the water surface

in the soil pores to the soil surface needs to be accounted for, even for thin soil layers (Kondo et al. (1990), Lee and Pielke (1992), Wu et al. (2000)). Indeed, in our own global and point simulations, we found excessive soil evaporation (not shown). To account for this we added an additional soil resistance term R_{soil} based on work by Sellers et al. (1992)

$$R_{soil} = (1 - f_{sno}) \exp(8.206 - 4.255s_1) \quad (F5)$$

where f_{sno} is the fractional soil covered by snow and s_1 is the soil moisture of the top layer relative to saturation determined from

$$s_1 = \frac{\theta_{ice,1} + \theta_{liq,1}}{\theta_{sat,1}} \leq 1 \quad (F6)$$

where $\theta_{ice,1}$, $\theta_{liq,1}$, and $\theta_{sat,1}$ are the volumetric ice, liquid water, and saturation water contents.

R_{soil} is set to zero in the case of dewfall.

Appendix G: Nitrogen limitation

PFT-dependent scale factors to represent nitrogen limitations on plant productivity were derived from a simulation with CLM coupled to a carbon/nitrogen cycle (CLM-CN, Thornton and Zimmerman 2007, Thornton et al. 2007). The factor, $f(N)$, represents the proportion of potential photosynthesis (gross primary production, or GPP) that is realized in the face of nitrogen limitation, as predicted by CLM-CN, for each PFT (Table G1). The simulation from which these factors are derived is a fully spun-up pre-industrial state, driven by 25-year cyclic NCEP drivers (1949-1972). The $f(N)$ is imposed on the maximum rate of carboxylation V_{max} in a manner similar to plant water stress (Oleson et al. 2004) as

$$V_{max} = V_{max25} (a_{vmax})^{\frac{T_v - 25}{10}} f(T_v) \beta_f f(N) \quad (G1)$$

where $V_{\max 25}$ is the value at 25°C ($\mu \text{ mol CO}_2 \text{ m}^{-2} \text{ s}^{-1}$), $a_{v \max}$ is the Q_{10} parameter, T_v is leaf temperature (C), $f(T_v)$ is a function that mimics thermal breakdown of metabolic processes, and β_i is a soil moisture limitation function.

CLM3.5 coupled to the DGVM is also over productive due to the switch from the CLM3 single-leaf to the new two-leaf model, which works optimally with CLM-CN. The DGVM was calibrated using the single-leaf model. With the two-leaf model the CLM3.5-DGVM simulates very high LAI and net primary production (NPP) and very fast tree growth. It also overestimates tree cover at the expense of grasses and grasses at the expense of bare ground. Despite this, the CLM3.5-DGVM PFT distributions look better, generally speaking, than the CLM3-DGVM distributions due to the improved simulation of the hydrological cycle. Some calibration of $f(N)$ has been performed with CLM3.5-DGVM (Table G1). However, LAI and NPP remain overestimated. Most PFT distributions look better than with the default values. However, the complex competition between boreal needleleaf evergreen and boreal deciduous trees as simulated with prior versions of CLM is difficult to reproduce. We have chosen to refrain from further model calibration at this point. Users may adjust the values in Table G1 as they see fit for their modeling purposes. In later version of CLM, the DGVM is intended to operate in tandem with the CN model, which should help overcome these problems.

REFERENCES

- Beven, K.J., and M.J. Kirkby (1979), A physically based, variable contributing model of basin hydrology, *Hydrol. Sci. Bull.*, *24*, 43-69.
- Bonan, G.B., S. Levis, L. Kergoat, and K.W. Oleson (2002), Landscapes as patches of plant functional types: An integrating concept for climate and ecosystem models, *Global Biogeochem. Cycles*, *16*, doi:10.1029/2000GB001360.
- Bonan, G.B., and S. Levis (2006), Evaluating aspects of the Community Land and Atmosphere Models (CLM3 and CAM3) using a dynamic global vegetation model, *J. Climate*, *19*, 2290-2301.
- Choudhury, B.J., N.E. DiGirolamo, J. Susskind, W.L. Darnell, S.K. Gupta, and G. Asrar (1998), A biophysical process-based estimate of global land surface evaporation using satellite and ancillary data II. Regional and global patterns of seasonal and annual variations, *J. Hydrology*, *205*, 186-204.
- Clapp, R.B., and G.M. Hornberger (1978), Empirical equations for some soil hydraulic properties, *Water Resour. Res.*, *14*, 601-604.
- Cosby, B.J., G.M. Hornberger, R.B. Clapp, and T.R. Ginn (1984), A statistical exploration of the relationships of soil moisture characteristics to the physical properties of soils, *Water Resour. Res.*, *20*, 682-690.
- Collins, W.D., et al. (2006), The Community Climate System Model version 3 (CCSM3), *J. Climate*, *19*, 2122-2143.
- Decker, M., and X. Zeng (2006), An empirical formulation of soil ice fraction based on in situ observations, *Geophys. Res. Lett.*, *33*, L05402, doi:10.1029/2005GL024914.

- Dickinson, R.E., A. Henderson-Sellers, and P.J. Kennedy (1993), Biosphere-Atmosphere Transfer Scheme (BATS) version 1e as coupled to the NCAR Community Climate Model, *NCAR Technical Note NCAR/TN-387+STR*, National Center for Atmospheric Research, Boulder, CO.
- Dickinson, R.E., K.W. Oleson, G. Bonan, F. Hoffman, P. Thornton, M. Vertenstein, Z.-L. Yang, and X. Zeng (2006), The Community Land Model and its climate statistics as a component of the Community Climate System Model, *J. Climate*, *19*, 2302-2324.
- Dirmeyer, P.A., X.Gao, M. Zhao, Z. Guo, T. Oki, and N. Hanasaki (2006), Multimodel analysis and implications for our perception of the land surface, *Bull. Amer. Meteorol. Soc.*, *87*, 1381-1397.
- Entekabi, D., and P.S. Eagleson (1989), Land surface hydrology parameterization for atmospheric general circulation models including subgrid scale spatial variability, *J. Climate*, *2*, 816-831.
- Hack, J.J., J.M. Caron, S.G. Yeager, K.W. Oleson, M.M. Holland, J.E. Truesdale, and P.J. Rasch (2006), Simulation of the global hydrological cycle in the CCSM Community Atmosphere Model version 3 (CAM3): mean features, *J. Climate*, *19*, 2199-2221.
- Kondo, J., N. Saigusa, and T. Sato (1990), A parameterization of evaporation from bare soil surfaces, *J. Appl. Meteorol.*, *29*, 385-389.
- Lawrence, D.M., P.E. Thornton, K.W. Oleson, and G.B. Bonan (2007), The partitioning of evapotranspiration into transpiration, soil evaporation, and canopy evaporation in a GCM: Impacts on land-atmosphere interaction, *J. Hydrometeorol.*, in press.
- Lawrence, P.J., and T.N. Chase (2007), Representing a new MODIS consistent land surface in the Community Land Model (CLM3.0), *J. Geophys. Res.*, in press.

- Lee, T.J., and R.A. Pielke (1992), Estimating the soil surface specific humidity, *J. Appl. Meteorol.*, 31, 480-484.
- Levis, S., G.B. Bonan, M. Vertenstein, and K.W. Oleson (2004), The Community Land Model's Dynamic Global Vegetation Model (CLM-DGVM): Technical description and user's guide, *NCAR Technical Note NCAR/TN-459+IA*, 50 pp., National Center for Atmospheric Research, Boulder, CO.
- Niu, G.-Y., Z.-L. Yang, R.E. Dickinson, and L.E. Gulden (2005), A simple TOPMODEL-based runoff parameterization (SIMTOP) for use in global climate models, *J. Geophys. Res.*, 110, D21106, doi:10.1029/2005JD006111.
- Niu, G.-Y., and Z.-L. Yang (2006), Effects of frozen soil on snowmelt runoff and soil water storage at a continental scale, *J. Hydrometeorol.*, 7, 937-952.
- Niu, G.-Y., Z.-L. Yang, R.E. Dickinson, L.E. Gulden, and H. Su (2007), Development of a simple groundwater model for use in climate models and evaluation with GRACE data, *J. Geophys. Res.*, doi:10.1029/2006JD007522, in press.
- Oleson, K.W., Y. Dai et al. (2004), Technical description of the Community Land Model (CLM), *NCAR Technical Note NCAR/TN-461+STR*, 173 pp., National Center for Atmospheric Research, Boulder, CO.
- Oleson, K.W., G.-Y. Niu, Z.-L. Yang, D.M. Lawrence, P.E. Thornton, P.J. Lawrence, R. Stockli, R.E. Dickinson, G.B. Bonan, and S. Levis, 2007: Improvements to the hydrological cycle in the Community Land Model and their impact on climate and vegetation biogeography, *J. Geophys. Res.*, in preparation
- Philip, J.R. (1957), Evaporation, and moisture and heat fields in the soil, *J. Meteor.*, 14, 354-366.

- Qian, T., A. Dai, K.E. Trenberth, and K.W. Oleson (2006), Simulation of global land surface conditions from 1948 to 2004: Part I: Forcing data and evaluations, *J. Hydrometeorol.*, 7, 953-975.
- Sellers, P.J., M.D. Heiser, and F.G. Hall (1992), Relations between surface conductance and spectral vegetation indices at intermediate (100 m² to 15 km²) length scales, *J. Geophys. Res.*, 97, D17, 19,033-19,059.
- Stockli, R., D. Lawrence, K.W. Oleson, P. Thornton, S. Denning, and G. Bonan (2007), A process-based evaluation of the new CLM3 hydrology by use of FLUXNET towers, *J. Geophys. Res.*, in preparation.
- Thornton, P.E., and N.E. Zimmermann (2007), An improved canopy integration scheme for a land surface model with prognostic canopy structure, *J. Climate*, in press.
- Thornton, P.E., J.-F. Lamarque, N.A. Rosenbloom, and N. Mahowald (2007), Effects of terrestrial carbon-nitrogen cycle coupling on climate-carbon cycle dynamics, *Global Biogeochem. Cycles*, in press.
- Wetzel, P.J., and J.T. Chang (1987), Concerning the relationship between evaporation and soil moisture, *J. Clim. Appl. Meteorol.*, 26, 18-27.
- White, M.A., P.E. Thornton, S.W. Running, and R.R. Nemani (2000), Parameterization and sensitivity analysis of the BIOME-BGC terrestrial ecosystem model: net primary production controls, *Earth Interactions*, 4, 1-85.
- Wu, A., T.A. Black, D.L. Versegny, M.D. Novak, and W.G. Bailey (2000), Testing the α and β methods of estimating evaporation from bare and vegetated surfaces in CLASS, *Atmos.-Ocean*, 38, 15-35.

- Yang, Z.-L., R.E. Dickinson, A. Henderson-Sellers, and A.J. Pitman (1995), Preliminary study of spin-up processes in land surface models with the first stage data of Project for Intercomparison of Land Surface Parameterization Schemes Phase 1(a), *J. Geophys. Res.*, *100*, 16,553-16,578.
- Yi, S., M. A. Arain, and M.-K. Woo (2006), Modifications of a land surface scheme for improved simulation of ground freeze-thaw in northern environments, *Geophys. Res. Lett.*, *33*, L13501, doi:10.1029/2006GL026340.

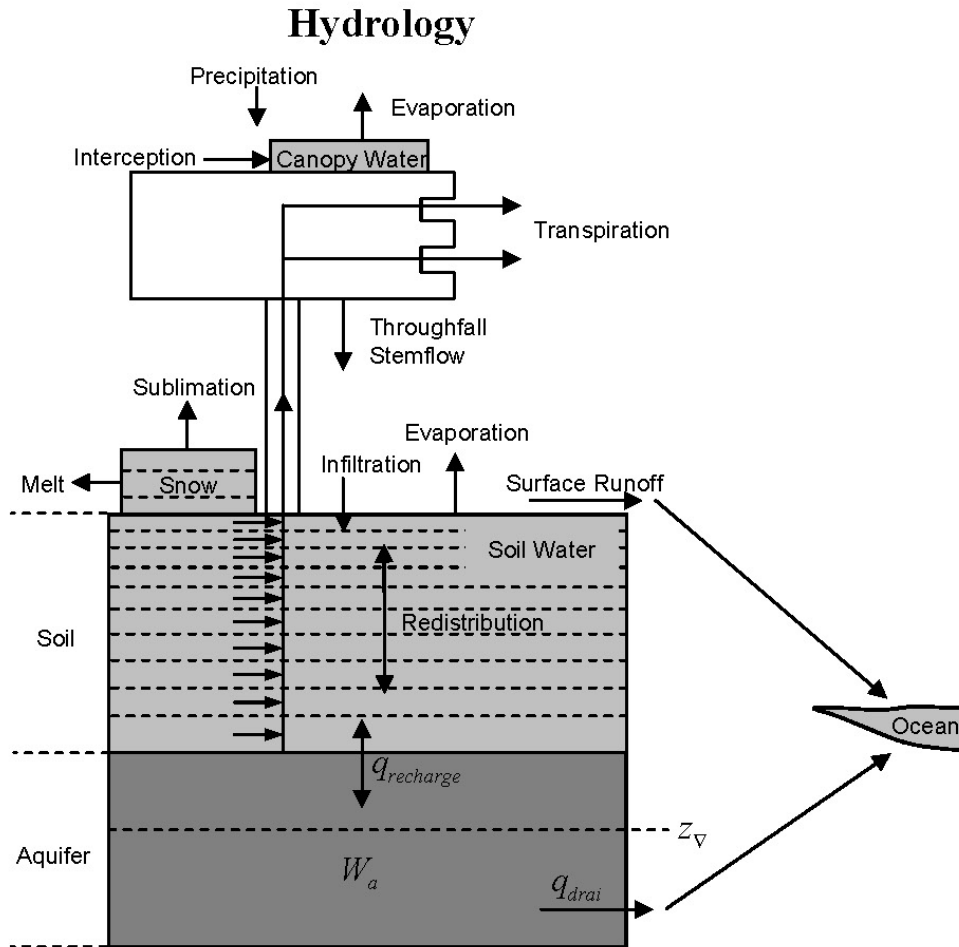


Figure C1. Hydrologic processes simulated by CLM3.5. An unconfined aquifer is added to the bottom of the CLM3 soil column (Niu et al. 2007). The depth to the water table is z_v (m). Changes in aquifer water content W_a (mm) are controlled by the balance between drainage from the aquifer water q_{drai} and the aquifer recharge rate $q_{recharge}$ ($\text{kg m}^{-2} \text{s}^{-1}$) (defined as positive from soil to aquifer).

TABLE E1. Soil water potential at full stomatal opening (ψ_{open}) and at full stomatal closure (ψ_{close}) for plant functional types.

Plant functional type	ψ_{open} ($\times 10^5$ mm)	ψ_{close} ($\times 10^5$ mm)
¹ Needleleaf evergreen tree – temperate	-0.66	-2.55
¹ Needleleaf evergreen tree – boreal	-0.66	-2.55
² Needleleaf deciduous tree – boreal	-0.66	-2.55
² Broadleaf evergreen tree – tropical	-0.66	-2.55
² Broadleaf evergreen tree – temperate	-0.66	-2.55
¹ Broadleaf deciduous tree – tropical	-0.35	-2.24
¹ Broadleaf deciduous tree – temperate	-0.35	-2.24
¹ Broadleaf deciduous tree – boreal	-0.35	-2.24
¹ Broadleaf evergreen shrub – temperate	-0.83	-4.28
¹ Broadleaf deciduous shrub – temperate	-0.83	-4.28
¹ Broadleaf deciduous shrub – boreal	-0.83	-4.28
¹ C ₃ arctic grass	-0.74	-2.75
¹ C ₃ grass	-0.74	-2.75
¹ C ₄ grass	-0.74	-2.75
³ Crop1	-0.74	-2.75
^{3,6} Crop2	-0.74	-2.75

¹White et al. (2000).

²Assigned values of needleleaf evergreen tree.

³Assigned values of grass.

⁶Two types of crops are specified to account for the different physiology of crops, but currently only the first crop type is specified in the surface dataset.

TABLE G1. Nitrogen limitation factor for plant functional types.

Plant functional type	$f(N)$	
	CLM3.5	CLM3.5-DGVM
Needleleaf evergreen tree – temperate	0.72	0.63
Needleleaf evergreen tree – boreal	0.78	0.62
¹ Needleleaf deciduous tree – boreal	0.79	-
Broadleaf evergreen tree – tropical	0.83	0.69
Broadleaf evergreen tree – temperate	0.71	0.35
Broadleaf deciduous tree – tropical	0.66	0.31
Broadleaf deciduous tree – temperate	0.64	0.36
Broadleaf deciduous tree – boreal	0.70	0.41
² Broadleaf evergreen shrub – temperate	0.62	-
² Broadleaf deciduous shrub – temperate	0.60	-
² Broadleaf deciduous shrub – boreal	0.76	-
C ₃ arctic grass	0.68	0.39
C ₃ grass	0.61	0.24
C ₄ grass	0.64	0.24
² Crop1	0.61	-
^{2,3} Crop2	0.61	-

¹Boreal needleleaf and broadleaf deciduous trees are merged into one PFT in CLM-DGVM (Levis et al. 2004).

²Shrubs and crops are not simulated in CLM-DGVM (Levis et al. 2004).

³Two types of crops are specified to account for the different physiology of crops, but currently only the first crop type is specified in the surface dataset.